A Novel Aperture-Loaded Decoupling Concept for Patch Antenna Arrays

Zhang, Yiming; Zhang, Shuai

Published in:
I E E E Transactions on Microwave Theory and Techniques

DOI (link to publication from Publisher):
10.1109/TMTT.2021.3085904

Publication date:
2021

Document Version
Accepted author manuscript, peer reviewed version

A Novel Aperture-Loaded Decoupling Concept for Patch Antenna Arrays

Yi-Ming Zhang, *Member, IEEE*, and Shuai Zhang, *Senior Member, IEEE*

***Abstract*—In this article, a novel decoupling approach is proposed for large-scale patch antenna arrays. With the additional coupling path from the feeding line of an element to its adjacent element through a small aperture, the mutual coupling between the two elements can be well canceled. Completely different from the traditional transmission-line-based decoupling methods, the proposed approach does not employ direct transmission/coupling bridges between the feeding lines of the elements. Besides, there is no additional impedance matching network, resulting in a simple design procedure. For verification purposes, a decoupled dual-polarized 1×8 linear antenna array is developed and tested. Results denote that both E- and H-plane coupling are suppressed to less than −30 dB at the center frequency of 4.9 GHz. To further improve the decoupling bandwidth, a magnitude-compensation technique using a dual-aperture configuration is developed. A design example of a 4×4 single-polarized patch antenna array integrated with the decoupling method is measured. The results depict that the array is well-decoupled within the band from 4.7 to 5.04 GHz, with an isolation level of over 24.7 dB. The proposed decoupling approach features simple implementation, low profile, with almost no influence on element radiation performance, and can be utilized for two-dimension large-scale arrays.**

***Index Terms*—Decoupling aperture, dual-polarization, large-scale array, magnitude compensation, transmission line.**

I. Introduction

In the past decade, increasing efforts have been devoted to canceling or suppressing the mutual coupling among antenna elements in antenna arrays, for instance, multiple-input multiple-output (MIMO) arrays, massive MIMO arrays, and phased arrays. For a small-scale MIMO array consisting of only two, three, or four antenna elements, a 17-dB in-band isolation level is high enough for MIMO communication, from the total efficiency and envelope correlation coefficient point of view [1]-[6]. However, a much higher isolation level is critical and essential in massive MIMO array systems since additional key performance is involved during beam scanning conditions. For a massive MIMO antenna array, to obtain good active impedance matching responses of the antenna elements, to keep the linearity and efficiency of the subsequently connected power amplifiers, and to finally realize a wide beam scanning range, the antenna elements should be positioned with a small distance and meanwhile the mutual coupling among antennas should be suppressed to less than −25 dB, or even lower [7]-[12]. Notice that when a massive MIMO array is working under beam scanning conditions, a large number of antenna elements, are excited simultaneously with specified excitation settings to achieve desired beam direction with high realized gain. Thus, the decoupling of a massive MIMO antenna array does not aim at the increasing of single element gain, but mainly focuses on keeping the peak gain being stable, avoiding dramatic gain rolloff during beam scanning, and maintaining good power amplifier linearity.

In general, there are four aspects of decoupling methods, categorized by the physical active areas: *a)* loading decoupling surfaces above the antenna apertures [10], [13]-[15], *b)* introducing decoupling resonators, electromagnetic band gap structures, or dummy elements in between antenna elements [11], [16]-[20], *c)* etching or adding decoupling structures on the ground plane of the antennas [21]-[23], and *d)* utilizing decoupling networks at feeding layers [2]-[6], [12], [24]-[28].

For the decoupling-surface-based methods, bulky system dimensions are generally required. For instance, the decoupling surfaces proposed in [10] and [13] should be positioned one quarter-wavelength away from the antenna apertures. In [14], surfaces with decoupling resonators were studied for linear antenna arrays. The surfaces were placed close to the antennas, however, the operating frequency of the antenna elements would offset from the original frequency.

Inserting dummy elements or decoupling resonators between antenna elements or at ground planes have been widely studied for small-scale arrays [16]-[18], [22]. Owing to the limited space among the antennas and the more complicated mutual coupling responses, the aforementioned methods are generally no longer satisfactory for large-scale arrays. More recently, some novel decoupling methods operating at the antenna aperture layer have been presented [11], [19], [20], [23]. In [11], wavetrap-based decoupling structures were studied for 45°-polarized patch antenna arrays. Considering the omnidirectional radiation characteristics of the wavetraps, the proposed decoupling structure does not work for dual-polarized arrays. In [23], a weak-field-decoupling method was proposed for probe-fed linear patch antenna arrays. This method works for an E-plane coupled array on the condition that the original coupling level should be very low of around −25 dB, and might be not effective for dual-polarized or two-dimension arrays.

This work was partially supported by Huawei project of "5G mmWave Decoupling Array". (*Corresponding author*: *Shuai Zhang*.)

The authors are with the Antenna, Propagation and Millimeter-wave Systems (APMS) Section, Department of Electronic Systems, Aalborg University, Denmark (e-mail: yiming@es.aau.dk, sz@es.aau.dk).

Compared to the above works, decoupling methods carried out at the feeding layer often have great advantages of the low profile, small influence on radiation performance of the elements as well as the applicability of different antenna configurations [2]-[6], [12], [26]-[28]. Notice that injecting additional signal to the desired node to cancel the parasitic effect is a common method in microwave network field. However, as for antenna decoupling, the challenge is how to achieve the target without influencing the radiation performance especially the realized gain and the cross-polarization level with a low profile and wide decoupling bandwidth. At this point, how to generate the additional decoupling path is the key point. For two- and three-element arrays, decoupling networks using *LC*- or distributed circuits have been investigated deeply [2]-[6], with normally additional impedance matching networks. However, in large-scale arrays, the coupling is more complicated and the leaking signals through different paths should be taken into consideration. In [12], a lattice-shaped decoupling network utilizing T-junction unequal power dividers was provided for two-dimension antenna arrays. The coupling between adjacent elements was canceled in a 4×4 patch antenna array, but a multi-layer configuration is essential for implementation with an intricate layout. In [27], a decoupling network loaded between the feeding points of the patch antennas was provided for linear arrays. The coupling paths among adjacent and nonadjacent elements are both suppressed. However, the aforementioned decoupling networks for large-scale arrays usually feature a narrow decoupling bandwidth due to the strong resonance of the transmission-line-based networks.

In this article, a novel decoupling concept by loading small apertures on the feeding line of every antenna element is proposed and investigated for large-scale antenna arrays. By introducing the additional coupling path from the feeding line to the adjacent element through the aperture, the strong coupling among the antenna arrays can be canceled. Specifically, a single-aperture decoupling method is firstly discussed for linear antenna arrays, to clearly show the basic operation of the decoupling scenario, as discussed in Section II and verified in Section III by giving a design example. Subsequently, to improve the decoupling bandwidth, a dual-aperture decoupling configuration is further provided, as investigated in Section IV with a design example shown in Section V. Comparison and extension discussions are provided in Section VI. Compared to the recently published decoupling methods, the novelty and the main contribution of this work are summarized as follows.

1) The decoupling apertures are of very small sizes and do not influence the cross-polarization level. This verifies the applicability of the proposed decoupling method for dual-polarized antenna arrays.

2) For the two-dimension array, both E- and H-plane coupling are canceled. With the contribution of the proposed magnitude-compensation method, the decoupling bandwidth is much wider compared to the ones of the published decoupling networks for large-scale arrays.

3) There is neither a direct decoupling bridge loaded between the feeding lines of adjacent elements nor the impedance matching network connected at the interface of every element, resulting in a simple design procedure.

4) The feeding lines are implemented in a single layer, avoiding the insertion loss from the transitions between different layers, leading to a low profile and compact layout.

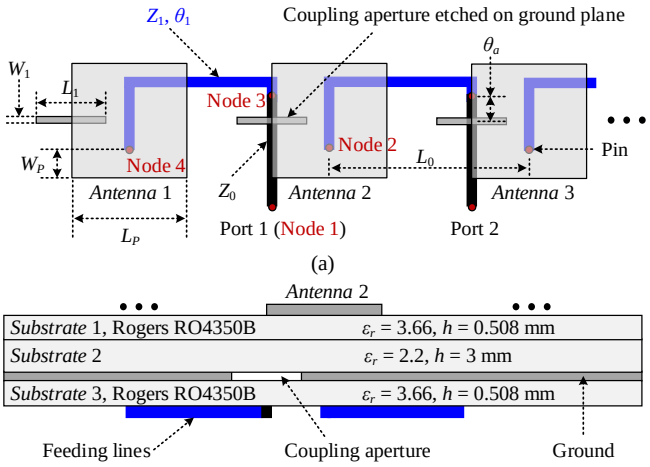

Fig. 1. Configuration of a H-plane-coupled linear antenna array integrated with the proposed decoupling method. (a) Top view, where L_0 = 30.6 mm, L_P = 16.8 mm, W_P = 4.6 mm. (b) Side view.

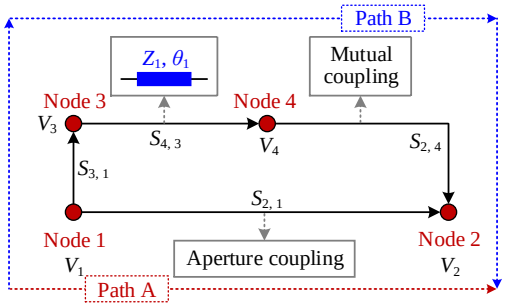

Fig. 2. Signal flow graph of the decoupling between Antennas 1 and 2.

II. Decoupling Principle

In this section, the basic decoupling principle of the proposed method will be investigated. Firstly, an H- and E-coupled linear antenna arrays integrated with the decoupling structures will be discussed respectively through the signal flow graph analysis in Part A. Subsequently, a decoupled dual-polarized antenna array will be further established and studied in Part B to show the performance of the proposed scheme.

A. Decoupling of single-polarized linear antenna arrays

Fig. 1 depicts an H-plane-coupled antenna array integrated with the proposed decoupling approach. For ease of analysis, patch antennas working at 4.9 GHz are utilized as the array elements in this article. The center distance between the adjacent element is set as $0.5\lambda_0$, where λ_0 is the free space wavelength at the center frequency. For every antenna element, a small coupling aperture is etched on the ground layer and loaded below the edge of the radiating patch. Here, taking antennas 1 (node 1) and 2 (node 2) as the study elements. The feeding line of antenna 1 is positioned across the aperture

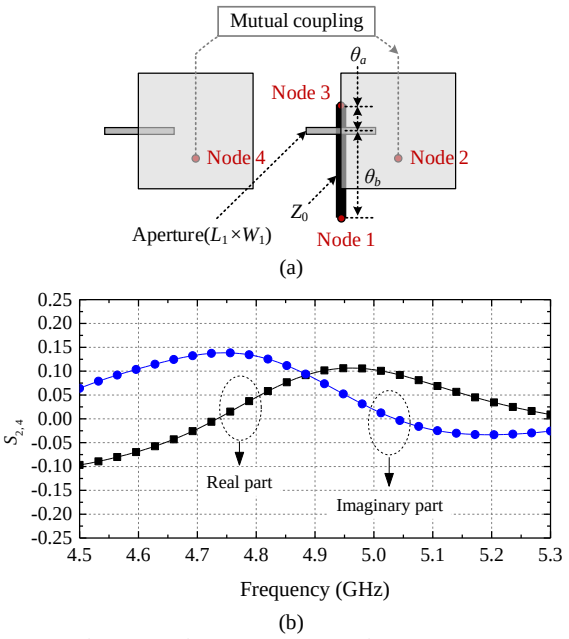

Fig. 3. (a) Configuration of the aperture-loaded four-port two-element antenna array for coupling analysis, where $\theta_a = 45°$, $\theta_b = 90°$. (b) Full-wave simulated mutual coupling level between nodes 4 and 2 without decoupling.

loaded under the adjacent antenna 2. The characteristic impedance of all the microstrip lines is set as Z_0 which equals the source and antenna impedance, except the one connecting the coupling aperture and the corresponding antenna element which is set as Z_1. Thereby, there are two coupling paths between adjacent antenna elements, i.e. aperture coupling and mutual coupling between radiating patches. By tuning the dimensions of the coupling aperture, the coupling level between nodes 1 and 2 through the aperture can be adjusted. With specified sizes (L_1 and W_1) of the aperture and the value of θ_1, the signals leaking from node 1 to node 2 through the two coupling paths can be optimized with identical magnitude and out of phase, leading to a well-decoupled response between antennas 1 and 2. Next, network analysis is carried out to describe the decoupling principle and the determination of the parameters in more detail.

Fig. 2 shows the signal flow graph of the decoupling between antennas 1 and 2, involving the loaded-aperture coupling and the mutual coupling among the patches, marked as Path A and Path B, respectively. Defining that the input voltage at node 1 is V_1, the output voltages at node 2 through the two paths can be expressed as [29]

$$V_{2,A} = S_{2,1}V_1 \tag{1a}$$

$$V_{2,B} = S_{3,1}S_{4,3}S_{2,4}V_1 \tag{1b}$$

where the parameters $S_{2,1}$ and $S_{2,4}$ represent the coupling levels of the paths through the loaded aperture and the mutual coupling among the radiating patches correspondingly. Based on the transmission line theory, we have

$$S_{4,3} = \frac{2Z_0Z_1}{2Z_0Z_1\cos\theta_1 + j(Z_0^2 + Z_1^2)\sin\theta_1} \tag{2}$$

For decoupling between nodes 1 and 2, we have that

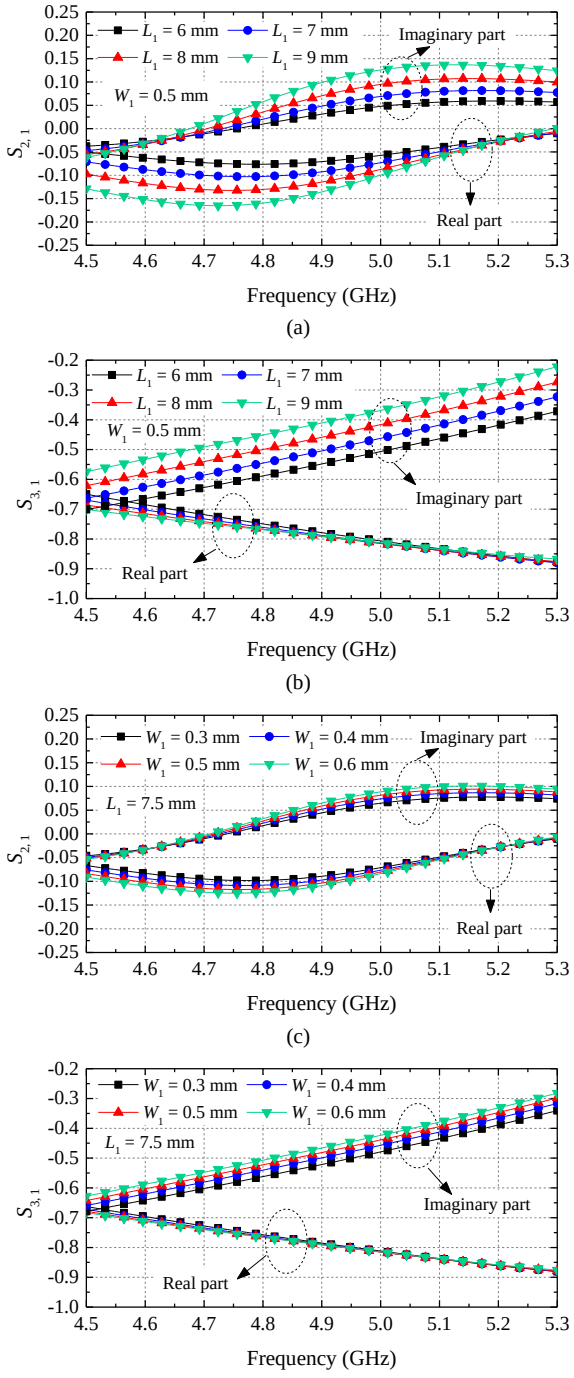

Fig. 4. Full-wave simulated transmission responses of the model shown in Fig. 3 with different dimensions of the aperture. (a) $S_{2,1}$ versus L_1. (b) $S_{3,1}$ versus L_1. (c) $S_{2,1}$ versus W_1. (d) $S_{3,1}$ versus W_1.

$$V_2 = V_{2,A} + V_{2,B} = 0 \tag{3}$$

Substituting (1) and (2) into (3), the following design condition is derived

$$S_{2,1} + \frac{2Z_0Z_1S_{3,1}S_{2,4}}{2Z_0Z_1\cos\theta_1 + j(Z_0^2 + Z_1^2)\sin\theta_1} = 0 \tag{4}$$

The coupling between antennas 1 and 2, i.e. $S_{2,4}$, is generally fixed in a given array configuration and can be readily obtained

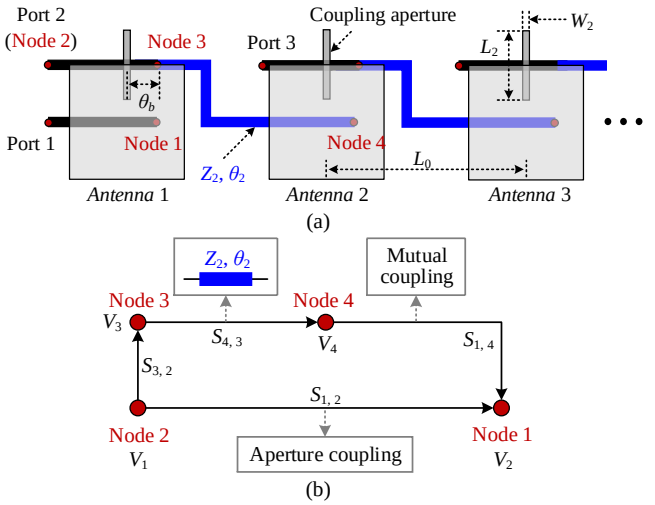

Fig. 5. (a) Configuration of an E-plane-coupled linear antenna array integrated with the proposed decoupling method. (b) Signal flow graph of the decoupling between Antennas 1 and 2.

through full-wave simulations. Therefore, it can be revealed from (4) that antennas 1 and 2 can be well decoupled. On the other hand, under the decoupled condition, the transmission line loaded cross the aperture (in between Node 1 and Node 3) can be considered as a two-port network, whose transmission matrix $abcd_1$ is also determined by the dimensions of the aperture and expressed as

$$abcd_1 = \begin{bmatrix} A_1 & B_1 \\ C_1 & D_1 \end{bmatrix} \tag{5}$$

For impedance matching purposes at Node 1, the following expression can be deduced

$$S_{1,1} = \frac{(P_1 - P_2)Z_1 \cos\theta_1 + j(P_3 - P_4)\sin\theta_1}{(P_1 + P_2)Z_1 \cos\theta_1 + j(P_3 + P_4)\sin\theta_1} = 0 \tag{6}$$

where

$$P_1 = A_1 Z_0 + B_1 \tag{7a}$$

$$P_2 = C_1 Z_0^2 + D_1 Z_0 \tag{7b}$$

$$P_3 = A_1 Z_1 + B_1 Z_0 \tag{7c}$$

$$P_4 = C_1 Z_0 Z_1^2 + D_1 Z_0^2 \tag{7d}$$

With the decoupling and impedance matching conditions deduced in (4) and (6), the dimensions of the aperture and the values of Z_1 and θ_1 can be determined.

To clarify the effects of the sizes of the aperture on the coupling level, a simplified four-port model is further constructed and analyzed, as illustrated in Fig. 3. The lengths of the transmission lines are fixed. Seeing that the mutual coupling level between the two radiating patches is relatively a small part of the total input signal as provided in Fig. 3(b), the energy leaking from node 1 to node 2 through the aperture should be also with a small level and close to the mutual coupling level. It is easily concluded that the transmission response from node 1 to node 2 should be changed by tuning the sizes of the aperture, as described in Fig. 4 where some representative results are summarized. The parameter study illustrated in Fig. 4 indicates that the larger the aperture is, the

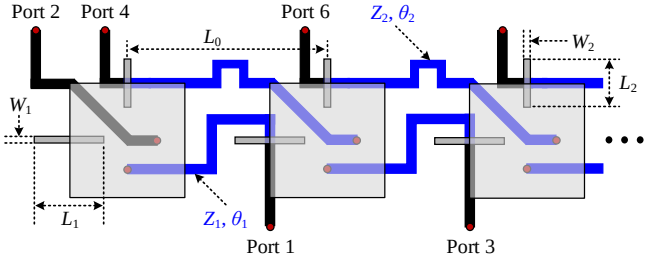

Fig. 6. Configuration of a dual-polarized linear antenna array integrated with the proposed decoupling method.

higher the aperture coupling level is. The real part of the transmission coefficient between node 1 and node 3, i.e. $S_{3,1}$, is almost not changed under different values of the length L_1 and the width W_1 of the aperture, as sketched in Figs. 4(b) and 4(d). Moreover, the analysis implies that the effect of the width on the coupling level is less sensitive than that of the length. This means that with a given value of the width, the aperture coupling level can be adjusted over a wide range by varying the length of the aperture. Based on the aforementioned discussions, the adjacent elements of the array shown in Fig. 1 can be readily decoupled under the condition of (4), where the parameters can be determined by carrying out the graphical studies provided in Fig. 4.

The above analysis has verified that the H-plane-coupled antenna array can be decoupled. As for the E-plane-coupled array, it can be easily concluded that the proposed decoupling method is still effective, as shown in Fig. 5 where the decoupling configuration and a signal flow graph are provided. By following the derivation and analysis for the array in Fig. 1, the dimensions of the aperture and the values of Z_2 and θ_2 can be determined. To describe the implementation of the proposed decoupling method, a simple design procedure is summarized, given as follows.

***Step A1*:** For a given antenna array, obtaining the mutual coupling matrices through full-wave simulations.

***Step A2*:** With a given value of the width of the aperture, determining the length of the aperture and the values of Z_1 and θ_1, based on (4), (6) and the graphical study shown in Fig. 4.

***Step A3*:** Determining the final layout through full-wave simulations and optimizations. In this step, all the situations in practical implementation should be taken into consideration, particularly avoiding the strong coupling between the transmission lines.

In this part, the decoupling principle of the presented method is studied. For decoupling purposes, only a small aperture is loaded for every patch antenna element. Notice that there is no direct decoupling operation for the non-adjacent elements in this work. As discussed that for adjacent elements, the coupling among the patches and the coupling going through the additional slot apertures would be canceled with each other at the radiating patch aperture. This implies that when a patch element is excited, the adjacent radiating patch aperture is the voltage-zero position after decoupling. The region around the adjacent radiating patch can be considered as the quasi-voltage-zero area. Subsequently, the surface wave and

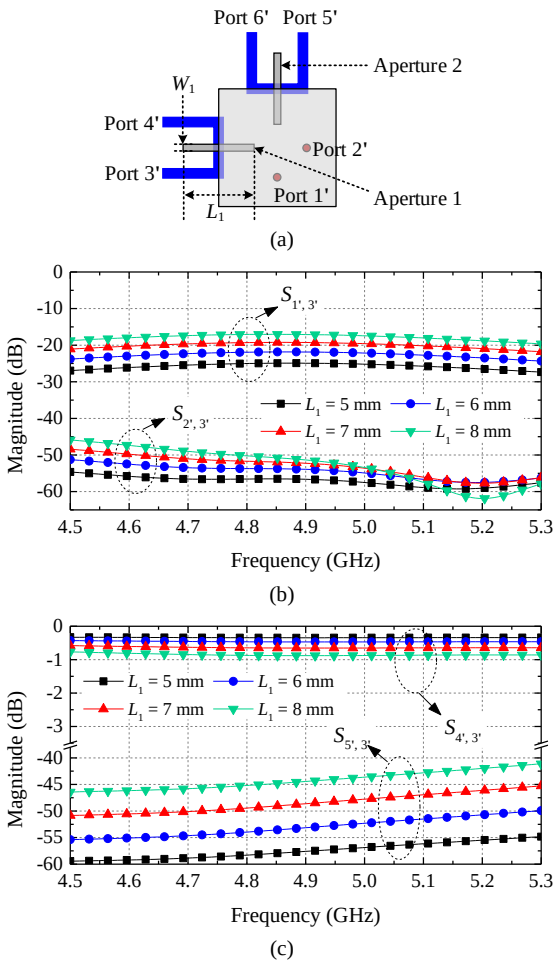

Fig. 7. (a) Simplified model of a dual-polarized antenna element with two aperture loaded for coupling analysis. (b) $S_{1',3'}$, $S_{2',3'}$, and (c) $S_{4',3'}$, $S_{5',3'}$ of the model with different dimensions of the coupling aperture.

free-space propagation from the excited patch to non-adjacent patches would be partially suppressed, leading to an improved non-adjacent isolation level. Compared to the other transmission-line-based decoupling approaches, there is no additional decoupling bridge or impedance matching network introduced in the proposed one, leading to a very simple decoupling structure.

B. Decoupling of dual-polarized linear antenna arrays

In Part A, the decoupling study of a single-polarized linear antenna array has been carried out. As for the decoupling of a dual-polarized antenna array, the array can be considered as a combination of two decoupled single-polarized subarrays. Since the coupling between orthogonal-polarized ports is already weak enough, it is much better to do nothing for these coupling paths. In this part, a dual-polarized linear antenna array integrated with the proposed decoupling method is constructed, as illustrated in Fig. 6. It is seen that two orthogonal apertures are loaded blow every radiating patch, and all the transmission lines are positioned on a single layer for low-profile and compactness purposes.

Before determining the parameters of the decoupling structures for the dual-polarized array, it is necessary to prove that the decoupling of the two groups (vertical- and horizontal-polarized groups) of co-polarized ports is independent of each other. Thus, a six-port model consisting of a dual-polarized element and two coupling apertures is established and studied, as shown in Fig. 7(a). Apertures 1 and 2 are employed for vertically- and horizontally-polarized ports, respectively. Below each aperture, a two-port transmission line is loaded. Taking port 3 as the representative port, the transmission coefficients between port 3 and other ports under different dimensions of aperture 1 is studied, as depicted in Fig. 7(b) and Fig. 7(c). The coupling level between ports 3 and 1 can be tuned to higher than −18 dB which is close to the mutual coupling level between adjacent elements without decoupling. Besides, the ones between ports 3 and 2, ports 3 and 5 are always at a very low level of less than −40 dB, as expected. This denotes that the decoupling between co-polarized ports has nearly no influence on the isolation level among orthogonal-polarized ports. According to the given design procedure, the parameters of the decoupled array shown in Fig. 6 are determined: $Z_0 = Z_1 = 50\ \Omega$, $\theta_1 = 271.4°$, $\theta_2 = 428.8°$, $L_1 = 7.6$ mm, $W_1 = 0.5$ mm, $L_2 = 5.4$ mm, $W_2 = 0.3$ mm.

In the next section, a decoupled dual-polarized antenna array is developed and measured to further verify the performance of the proposed decoupling method, including the comparisons of the arrays with and without decoupling.

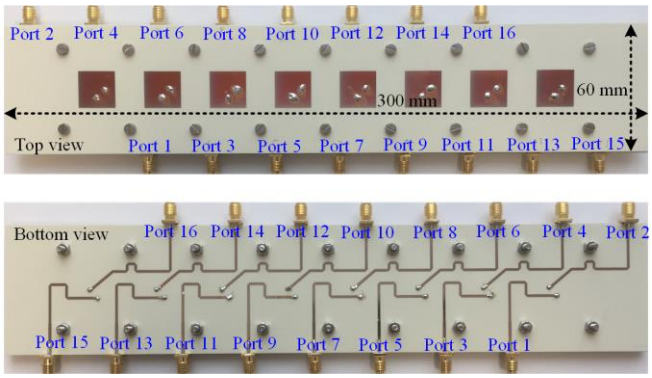

Fig. 8. Photos of the 1×8 dual-polarized antenna array using the proposed decoupling method.

III. Design Example A: A Decoupled Dual-Polarized Linear Antenna Array

For verification purposes, a 1×8 dual-polarized decoupled antenna array is fabricated and measured based on the scheme given in Fig. 6, as shown in Fig. 8. Some metal screws are used for fixation, whose positions have been carefully considered during full-wave simulations to make sure the influence on the decoupling performance can be negligible. The *S* parameters and the radiation performance of the decoupled array are fully tested by using the Agilent 85309N network analyzer and the SATIMO SG24L spherical near-field scanner, respectively.

Fig. 9 and Fig. 10 illustrate the reflection coefficients and coupling levels of some representative ports of the array with/without decoupling (i.e., Ports 7 and 8), respectively. It is verified from both simulated and measured results that the

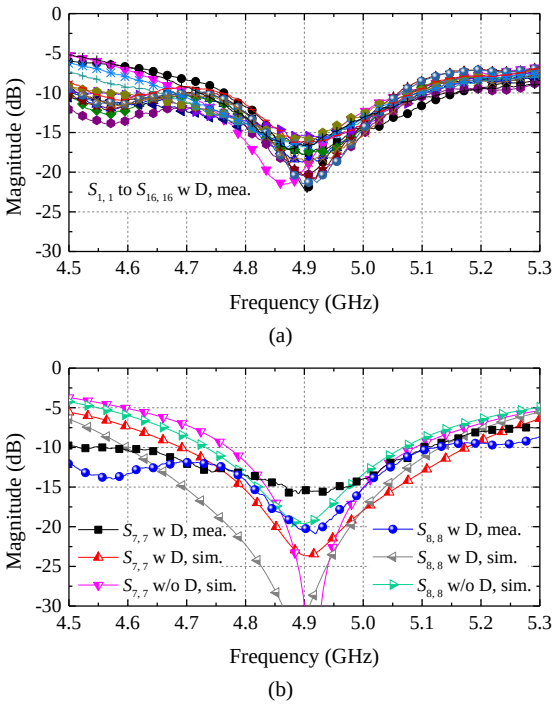

Fig. 9. Measured *S* parameters of the representative ports of the 1×8 array. (a) $S_{i,i}$. (b) $S_{7,7}$ and $S_{8,8}$.

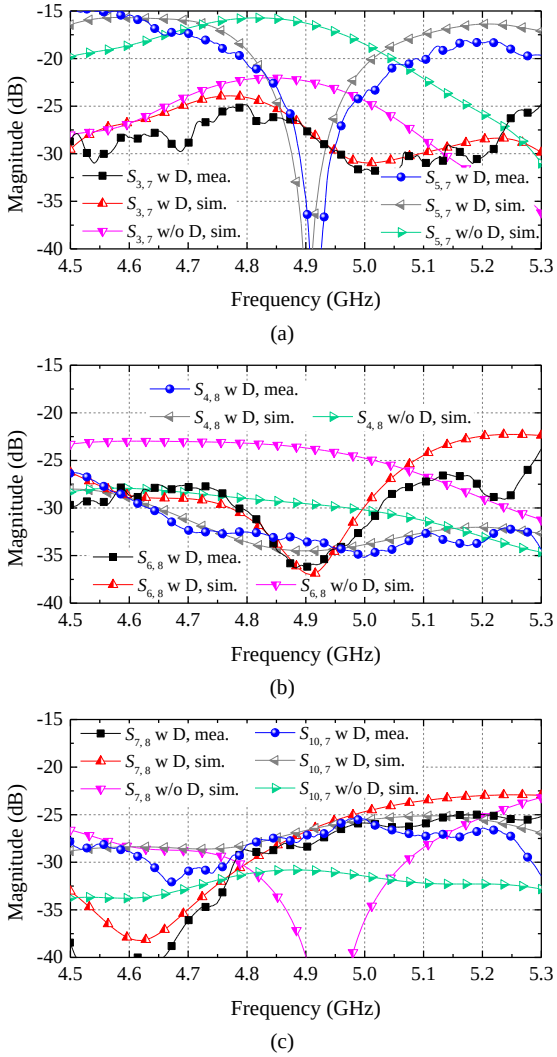

Fig. 10. Measured *S* parameters of the representative ports of the 1×8 array. (a) $S_{3,7}$ and $S_{5,7}$. (b) $S_{4,8}$ and $S_{6,8}$. (c) $S_{7,8}$ and $S_{10,7}$.

impedance bandwidth is broadened after decoupling without using any additional impedance matching solution. The measured results with decoupling show a better impedance matching response at the lower edge of the operating band, compared to the simulated ones. This is mainly due to the unideal touching between the different layers in the multi-layer antenna configuration, where some small air gaps may exist, leading to a slight influence on the input impedance of the antenna element in practice. For the ports with the vertical polarization, the in-band port-to-port isolation between adjacent elements, i.e. $S_{5,7}$, is significantly enhanced from 15.7 dB to higher than 30 dB around the center frequency. As for the isolation between non-adjacent ports, such as $S_{3,7}$, it is increased by around 5 dB. For the ports with the horizontal polarization, the coupling levels between adjacent and non-adjacent ports are suppressed to lower than −30 dB after decoupling, where the maximum coupling is higher than −23.2 dB before decoupling. Especially for the non-adjacent element, the original coupling level is lower than the one between adjacent elements, resulting in a wider decoupling bandwidth referring to a 25-dB isolation level. Notice that there is no decoupling consideration between the ports with orthogonal polarizations since the coupling level is normally low enough. It is seen from Fig. 10(b) that the mentioned coupling level is still kept below −25 dB with the proposed decoupling method, as expected.

Fig. 11 provides the radiation patterns of the arrays with and without decoupling. It is observed that the simulated ones after decoupling are almost the same as the ones before decoupling. This denotes that the proposed method has nearly no effect on the radiation pattern theoretically, including both co- and cross-polarized patterns. As for the measured results, they are mainly consistent with the simulated ones, except that the cross-polarization level is slightly higher than the simulated one, mainly due to the assembling error in practice. Despite this, the measured cross-polarization level is still kept at a low level. This further verifies that the proposed aperture-based decoupling structure is effective for dual-polarized antenna arrays, as discussed in Section II-B. The total efficiency and maximum realized gain are also measured, as plotted in Fig. 12. The proposed decoupling structure features a very small insertion loss, and the in-band total efficiency is almost higher than 80% after decoupling.

The aforementioned results denote that the antenna array integrated with the proposed decoupling aspect is well decoupled with a low insertion loss. On the other hand, observe that for the antenna ports with the H-plane coupling, the decoupling bandwidth still features a narrow response, as shown in Fig. 10(a). In the next section, a dual-aperture-based decoupling aspect will be further developed for compensating the magnitude imbalance between the aperture coupling path and the original space coupling among the radiating patches.

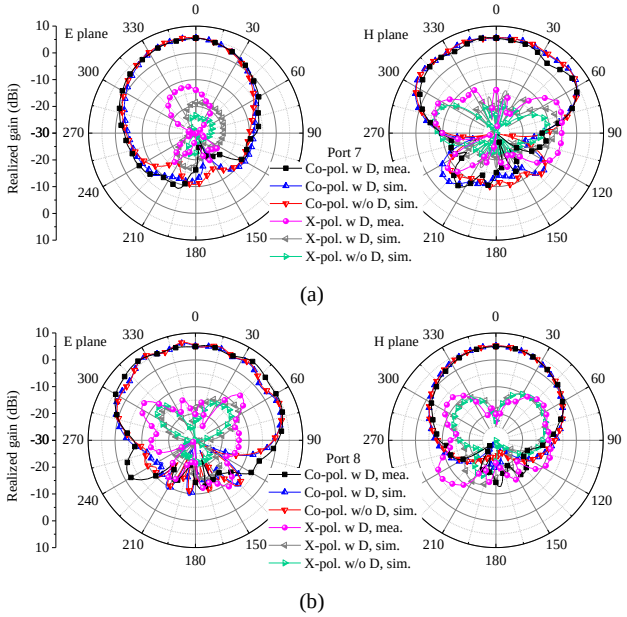

Fig. 11. Measured and simulated radiation patterns of the proposed 1×8 array with (a) Port 7 excited, and (b) Port 8 excited.

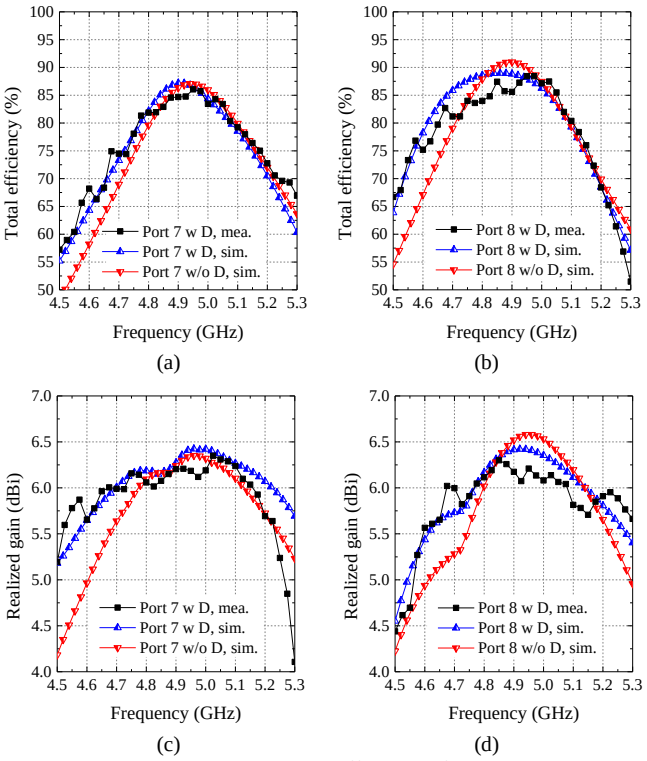

Fig. 12. Measured and simulated total efficiency of the proposed 1×8 array with (a) Port 7 excited, and (b) Port 8 excited. Maximum realized gain of the array with (c) Port 7 excited, and (d) Port 8 excited.

This magnitude-compensation method can then be utilized to improve the decoupling bandwidth.

IV. Decoupling of 2-Dimension Antenna Arrays

The performance of the linear antenna arrays using the proposed decoupling method has been verified based on the above discussions. In this section, an $M\times N$ antenna array

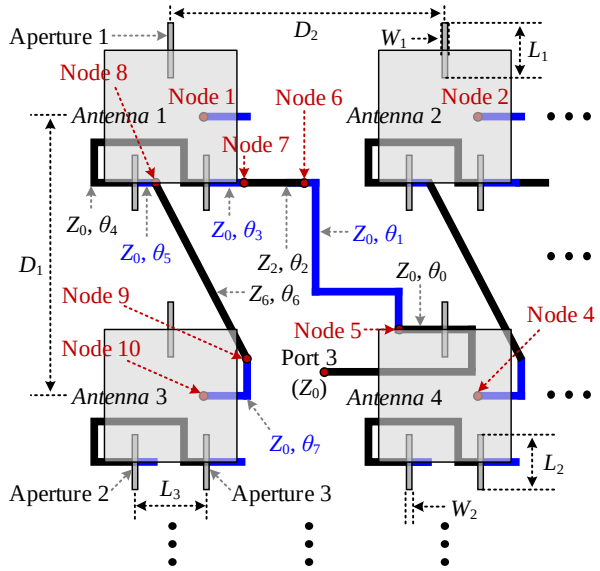

Fig. 13. Configuration of a two-dimension antenna array integrated with the proposed decoupling method. Port 3 (the input interface of antenna 3) is selected as the representative port.

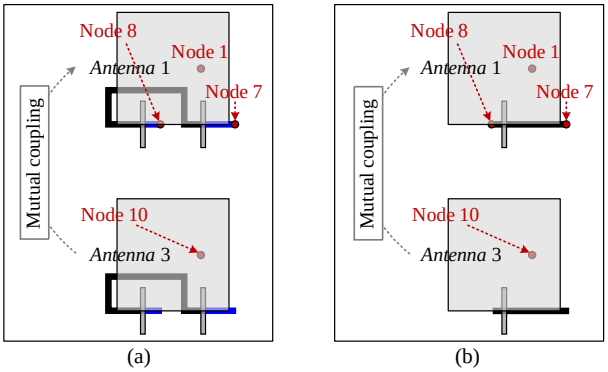

Fig. 14. Configurations of the two-element array with (a) dual-aperture coupling and (b) single-aperture coupling.

integrated with the aperture-loaded decoupling structures is further established and analyzed, as illustrated in Fig. 13. Here, port 3, which is the input interface of antenna 3, is selected as the representative port. Starting at port 3, the transmitting path passes through single-aperture and dual-aperture structures in turn, to cancel the coupling paths between antennas 3 and 4, antennas 3 and 1 correspondingly. Based on the discussion carried out in Section III, the decoupling bandwidth between H-plane-coupled antennas is narrower than the one between E-plane-coupled antennas by using a single-aperture decoupling method. Hereby, a dual-aperture-loaded approach is further proposed to achieve an improved decoupling bandwidth for H-plane-coupled antennas.

To clarify the compensation scheme more clearly, a comparison study between the dual- and single-aperture decoupling structures is carried out, where antennas 1 and 3 in Fig. 13 are selected. Figs. 14(a) and 14(b) illustrate the two-element H-plane coupled arrays loaded with dual- and single-aperture structures, respectively. For the two-element array without decoupling, the mutual coupling can be readily obtained by using full-wave simulations. To cancel the mutual

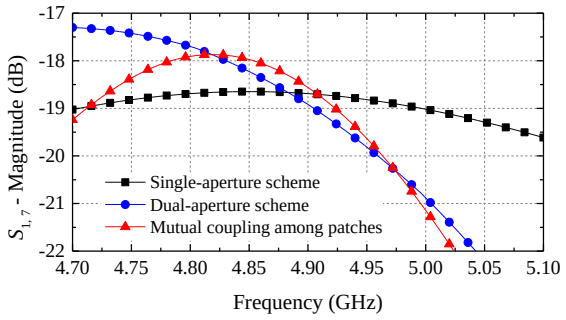

(a)

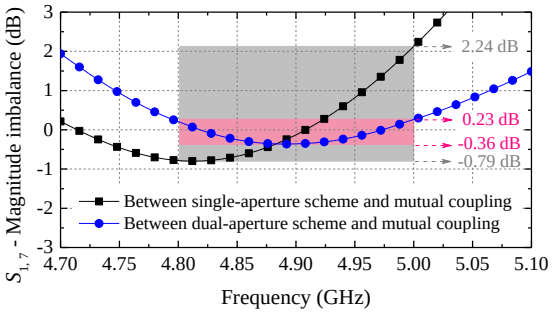

(b)

Fig. 15. Comparison of the coupling level using single- and dual-aperture schemes. (a) Magnitude level of the coupling between nodes 1 and 7. (b) Magnitude imbalance referred to the original mutual coupling level between nodes 1 and 10 without decoupling.

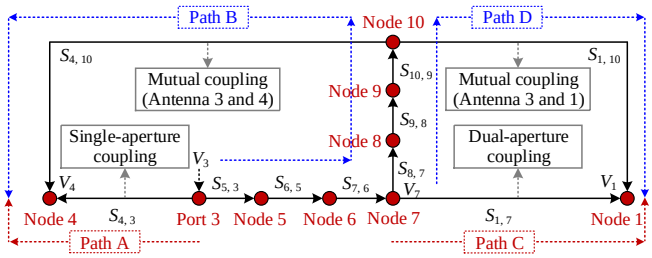

Fig. 16. Signal flow graph of the decoupling between antennas 1 and 2, antennas 2 and 4.

coupling, it is reasonably assumed that the coupling level between the transmission line and patch through the aperture-based structure should be close to the mutual coupling between the radiating patches. It is an easy matter to achieve the requirement at the center frequency 4.9 GHz, by using either the single- or dual-aperture schemes. However, the magnitude of the path through aperture coupling should be changed when the frequency departs from the center frequency, which might lead to a degradation in the decoupling level within the operating frequency band.

Fig. 15(a) shows the full-wave simulated coupling levels between nodes 1 and 7 of the arrays shown in Fig. 14, along with the original mutual coupling without decoupling. It is obtained that the coupling magnitudes of both the dual- and single-aperture decoupling schemes are close to the mutual coupling level at 4.9 GHz. With the single-aperture scheme, the magnitude imbalance between the aperture coupling and the original mutual coupling increases quickly as the frequency departs from 4.9 GHz. This leads to the fact that the decoupling response would feature a strong resonance and a narrow bandwidth, as verified in Fig. 10(a). As for the result obtained by using the dual-aperture scheme, a magnitude compensation is realized by selecting specified dimensions and positions of the apertures and the electrical length θ_4 loaded between the two apertures. Therefore, the magnitude imbalance is reduced compared to the case using the single-aperture scheme, indicating a potentially wider decoupling bandwidth. As seen from Fig. 15(b), the maximum magnitude imbalance is reduced from 2.24 dB to 0.36 dB by using the dual-aperture scheme, within the range from 4.8 to 5.0 GHz.

Similar to the aforementioned linear arrays, a signal flow graph of the two-dimension array is further established, as shown in Fig. 16. Defining that the input voltage at port 3 is V_3, the signals leaking through paths A and B should be canceled with each other at node 4 to cancel the coupling between antennas 3 and 4. This is the same for paths C and D for decoupling of antennas 3 and 1. Subsequently, based on the network analysis theory, the following equations can be derived under the decoupling conditions

$$V_A+V_B = S_{4,3}V_3+S_{5,3}S_{6,5}S_{7,6}S_{8,7}S_{9,8}S_{10,9}S_{4,10}V_3=0 \tag{8a}$$

$$V_C+V_D = S_{1,7}V_7+S_{8,7}S_{9,8}S_{10,9}S_{1,10}V_7=0 \tag{8b}$$

where

$$S_{6,5}=\cos\theta_1 - j\sin\theta_1 \tag{9a}$$

$$S_{7,6}=\frac{2Z_0}{2\cos\theta_2 + j\dfrac{Z_0^2+Z_2^2}{Z_0Z_2}\sin\theta_2} \tag{9b}$$

$$S_{9,8}=\frac{2Z_0}{2\cos\theta_6 + j\dfrac{Z_0^2+Z_6^2}{Z_0Z_6}\sin\theta_6} \tag{9c}$$

$$S_{10,9}=\cos\theta_7 - j\sin\theta_7 \tag{9d}$$

In (8), the S parameters $S_{1,10}$ and $S_{4,10}$ represent the mutual coupling among antennas 1 and 3, antennas 3 and 4, respectively. The rest S parameters that are not mentioned in (9a)-(9d) denote the transmission responses of the loaded aperture-coupled structures. Besides, the transmission matrix $abcd_2$ = [A_2, B_2, C_2, D_2] from Port 3 to Node 10 under decoupling condition can be derived as

$$abcd_2=\begin{bmatrix}A_3 & B_3\\ C_3 & D_3\end{bmatrix}\begin{bmatrix}\cos\theta_1 & jZ_0\sin\theta_1\\ \dfrac{j\sin\theta_1}{Z_0} & \cos\theta_1\end{bmatrix}\begin{bmatrix}\cos\theta_2 & jZ_2\sin\theta_2\\ \dfrac{j\sin\theta_2}{Z_2} & \cos\theta_2\end{bmatrix}$$
$$\times\begin{bmatrix}A_4 & B_4\\ C_4 & D_4\end{bmatrix}\begin{bmatrix}\cos\theta_6 & jZ_2\sin\theta_6\\ \dfrac{j\sin\theta_6}{Z_6} & \cos\theta_6\end{bmatrix} \tag{10}$$

where the matrices $ABCD_3$ and $ABCD_4$ represent the transmission performance from Port 3 to Node 5, and Node 7 to

TABLE I
PARAMETER VALUES OF THE DECOUPLED 4×4 ANTENNA ARRAY

D_1	D_2	L_1	W_1	L_2	W_2
36.7 mm	30.6 mm	6.4 mm	0.3 mm	7.8 mm	0.7 mm
L_3	Z_0	Z_2	Z_6	θ_0	θ_1
12 mm	50 Ω	82.5 Ω	74.8 Ω	22.6 °	445.6 °
θ_2	θ_3	θ_4	θ_5	θ_6	θ_7
135.7 °	13.8 °	320.7 °	18.3 °	267.5 °	51.1 °

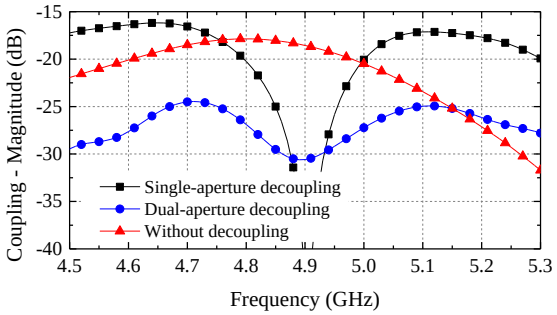

Fig. 17. Full-wave simulated isolation levels between antennas 1 and 3 with H-plane coupling using the dual- and single-aperture decoupling schemes as shown in Fig. 15.

Node 8 respectively, which are determined by the dimensions of the coupling apertures. For impedance matching purpose, we have that

$$S_{3,3} = \frac{A_2 Z_0 + B_2 - C_2 Z_0^2 - D_2 Z_0}{A_2 Z_0 + B_2 + C_2 Z_0^2 + D_2 Z_0} = 0 \qquad (11)$$

Note that the characteristic impedances of two transmission lines are set as Z_2 and Z_6 respectively, and the others are all 50-Ω transmission lines. The non-50-Ω lines contribute not only to achieve the target of decoupling but also to impedance matching improvement. By following the similar parameter studies given in Fig. 4, the values of the parameters including the characteristic impedance, electrical lengths, as well as physical dimensions of the apertures can be determined based on (8)-(11) for H-plane and E-plane decoupling. Despite that there is no direct decoupling between diagonal elements and non-adjacent elements, the related mutual coupling paths are also suppressed. This will be verified in the next section where a demonstrator is designed and measured.

To give an overview of the parameter determination of the developed dual-aperture-based decoupling method, a design procedure is summarized, given as follows.

***Step B1*:** For a given antenna array, extracting the mutual coupling matrices through full-wave simulations.

***Step B2*:** Determining the values of θ_3, θ_4, θ_5, and the dimensions of the dual-aperture structure, by following the magnitude imbalance study given in Figs. 13 and 14 to achieve the magnitude compensation purpose.

***Step B3*:** Determining the values of Z_6, θ_6, and θ_7, by following the relation given in (8b) to realize the H-plane decoupling. It should be mentioned that to determine the value of Z_6, the impedance matching at node 7 seen looking toward the antenna 3 is also considered.

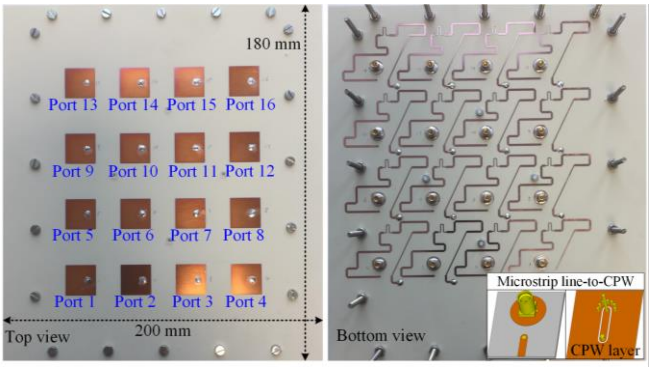

Fig. 18. Photos of the 4×4 antenna array using the proposed decoupling method.

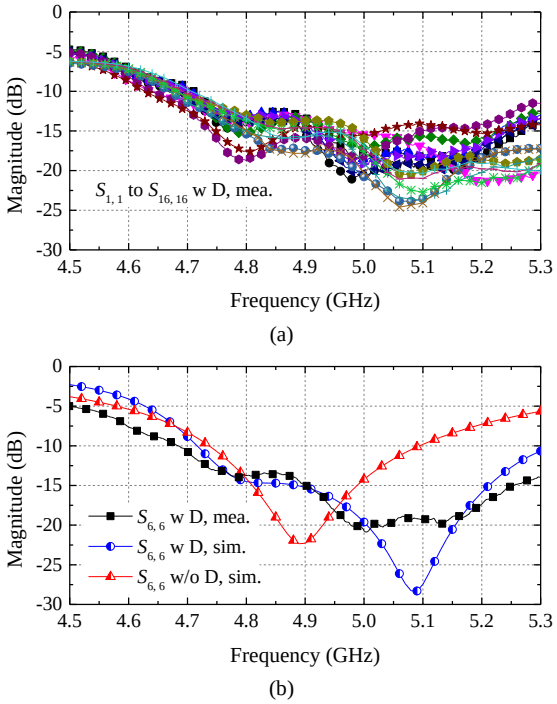

Fig. 19. Measured *S* parameters of the representative ports of the 4×4 array. (a) $S_{i,i}$. (b) $S_{6,6}$.

***Step B4*:** Determining the values of θ_0, θ_1, θ_2, Z_2, and the dimensions of the single-aperture structure based on (8a), to realize the E-plane decoupling. Particularly, this step can be achieved by referring the *steps A1-A3* given in Section II-A. Similar to Z_6, the impedance matching performance can be improved by selecting a proper value for Z_2.

***Step B5*:** Evaluating and checking whether the determined values of the parameters satisfy (11) or not. If not, a new group of the parameters should be reselected through steps *B3* and *B4* until they fit (11).

***Step B6*:** Determining the final layout through full-wave simulations and optimizations. In this step, all the situations in practical implementation should be taken into consideration, particularly avoiding the strong coupling between the transmission lines and the soldering pads of the connectors.

For a 4×4 antenna array using the configuration shown in Fig. 13, a group values of the parameters are determined, as listed in

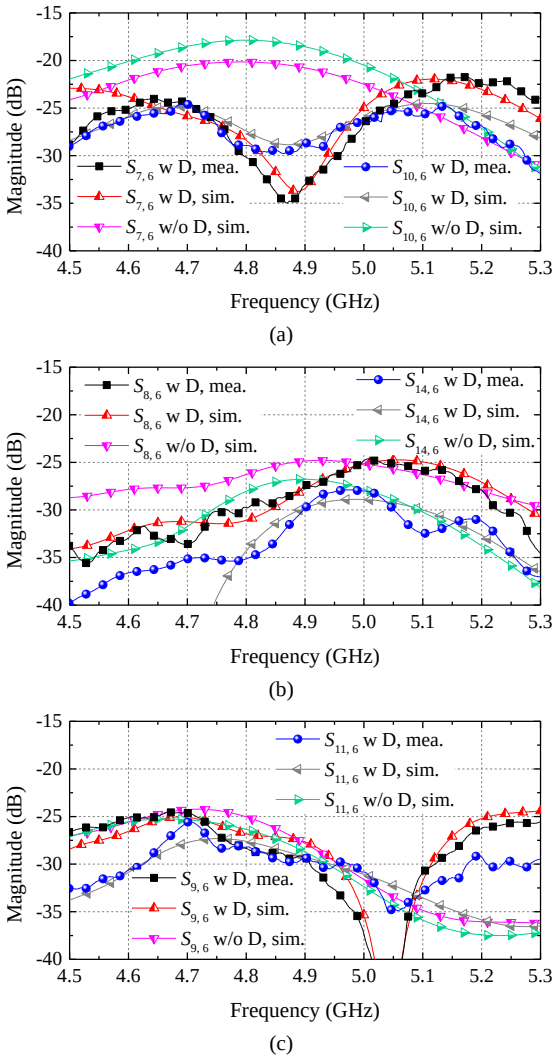

Fig. 20. Measured *S* parameters of the representative ports of the 4×4 array. (a) $S_{7,6}$ and $S_{10,6}$. (b) $S_{8,6}$ and $S_{14,6}$. (c) $S_{9,6}$ and $S_{11,6}$.

Table I. Fig. 17 plots the full-wave simulated results of the two-element arrays shown in Fig. 14 integrated with the dual-aperture decoupling structure based on the values given in Table I. With the help of the magnitude compensation of the dual-aperture structure, the mutual coupling level is suppressed to nearly −25 dB among the entire studied band. The result of the array using the single-aperture scheme is also provided, which increases dramatically when the frequency departs from 4.9 GHz, indicating a narrow decoupling bandwidth. Please note that as for the dual-aperture decoupled two-element array, a total efficiency drop of less than 3% (0.13 dB) is obtained compared to the single-aperture decoupled two-element array. This contributes only a 0.26-dB improvement to the isolation. In Section V, a demonstrator of a decoupled 4×4 antenna array will be further developed, measured, and discussed to verify the decoupling performance of the proposed method.

V. Design Example B: A Decoupled 4×4 Antenna Array

In this section, a 4×4 antenna array is designed and fabricated for demonstration purposes, as shown in Fig. 18. For ease of testing, microstrip line-to-CPW transitions are utilized for soldering the MMCX connectors, with a very small insertion loss of around 0.15 dB. The performance of the array is fully measured.

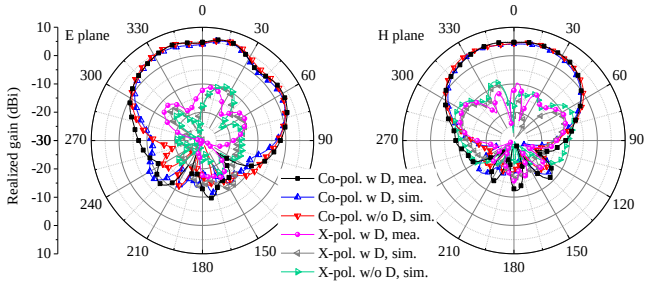

Fig. 21. Measured and simulated radiation patterns of the proposed 4×4 array with Port 6 excited.

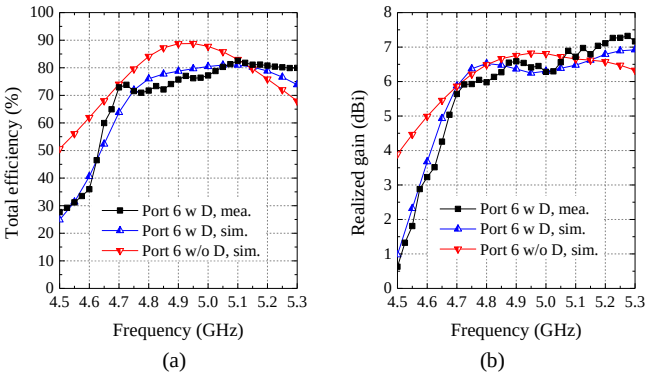

Fig. 22. Measured and simulated (a) total efficiency and (b) maximum realized gain of the proposed 4×4 array with Port 6 excited.

Fig. 19 and Fig. 20 illustrate the *S* parameters of the array where Port 6 is selected as the representative port. The impedance bandwidth is significantly enlarged by using the proposed decoupling method, without using any additional impedance matching structures. More detailed, the fractional bandwidth of the decoupled antenna is 12.6% from 4.68 to over 5.3 GHz, with the center frequency 4.9 GHz as the reference. It is also verified that for the adjacent elements, the maximum coupling level is significantly canceled to less than −24.7 dB, within the range from 4.7 to 5.04 GHz, representing the fractional bandwidth of over 7%. Particularly, the H-plane coupling, i.e. $S_{10,6}$, is suppressed by 7 dB among the entire study bandwidth, compared to the one of higher than −17.7 dB before decoupling. This is contributed by the proposed dual-aperture decoupling configuration. For the non-adjacent elements with the same polarization, the port-to-port coupling level is also suppressed from −24.9 dB to −27.8 dB around and lower than the center frequency, which is less than −25 dB within the study frequency range, as illustrated in Fig. 20(b). Other coupling paths that are not mentioned are still kept at a low level of less than −24.8 dB, which is not detailed for brevity. The radiation pattern, total efficiency, and the maximum realized gain of the decoupled array are provided in Figs. 21, 22(a), and 22(b), respectively. It is demonstrated from Fig. 21 that the radiation pattern has nearly no distortion after decoupling, and the measured and simulated results are

TABLE II
PERFORMANCE COMPARISONS AMONG SOME PUBLISHED FEEDING-LAYER-BASED AND THE PROPOSED DECOUPLING TECHNIQUES

Ref./Year	Antenna array configuration	Require additional impedance matching structure	Decoupling bandwidth*	In-band isolation improvement between adjacent elements	Isolation between non-adjacent elements	Decoupled total efficiency
[4]/2015	1×2@2.45 GHz Monopole arrays	Yes	9%~17%	11 dB (from 9 to 20 dB)	/	78.2%~81.2%
[5]/2017	1×2@0.75/1.25 GHz Monopole arrays	Yes	1.7%~5.3%	10~14 dB (from 6/10 to 20 dB)	/	67%~72%
[12]/2019**	4×4@4.9 GHz Patch array	Yes	1.8%	10 dB (from 15 to 25 dB)	≥ 24.3 dB	≥ 70%
[27]/2019	1×5@5.56 GHz E-coupled patch array	No	1.1%	6.6 dB (from 8.4 to 15 dB)	≥ 17 dB	Not given
This work	**4×4@4.9 GHz Patch array**	**No**	**7%**	**7 dB (from 17.7 to 24.7 dB)**	**≥ 24.8 dB**	**≥ 70.9%**

*denotes the fractional decoupling bandwidth with the condition that $|S_{1,1}| \leq -10$ dB.
**denotes the full-wave simulated result.

consistent with each other, including both the co- and cross-polarization patterns.

Observe that the total efficiency is degraded by the maximum level of around 15% at the center frequency, corresponding to an additional insertion loss of approximately 0.7 dB. This is mainly contributed by the loss of the microstrip lines and the microstrip line-to-CPW transition. The insertion loss is acceptable from large-scale antenna array applications point of view since the total efficiency is over 70.9% after decoupling. It is anticipated that by using the substrate materials with lower loss tangent values, the insertion loss should be reduced. The results provided in this section verify the decoupling performance of the antenna array integrated with the developed dual-aperture decoupling structure. Next, a comprehensive comparison study will be further operated to show the overview performance and advantages of the proposed decoupling concepts.

VI. COMPARISON AND EXTENSION STUDIES

Table II lists some recently published decoupling methods operated at the feeding network layer for comparison purposes. In [4] and [5], some decoupling networks were provided for monopole arrays. A wide decoupling bandwidth might be achieved as listed in the table, with a compact system size by using the Low Temperature Co-Fired Ceramic technique which leads to a high implementation cost. Moreover, additional impedance matching networks or structures are essential. These decoupling networks are effective for two-element arrays, but difficult to be extended for large-scale antenna arrays where the requirements for beam scanning should be taken into consideration, as explained in Section I. For massive MIMO antenna systems, it is very popular to use patch antennas as the array elements [10]-[15]. Compared to the aforementioned monopole arrays, it is much different to implement antenna decoupling at the feeding layer in large-scale arrays. One of the challenges is decoupling bandwidth improvement. In [12], a lattice-shaped decoupling network was presented for large-scale patch antenna arrays. A bulky impedance matching network using a three-order transformer was employed, and a narrow decoupling bandwidth of around 1.8% was finally obtained. In [27], a neutralization-line-based decoupling network was studied for linear antenna arrays. There was no additional impedance matching network, however, the realized decoupling bandwidth was relatively narrow of around 1.1%. As for the decoupled array proposed in this article, the common bandwidth for decoupling and impedance matching is over 7% without using additional impedance matching operation. All the coupling paths are well-suppressed or kept at a level of less than 24.7 dB. Despite that a small insertion loss is observed which is mainly due to the dielectric loss, the total efficiency of the antenna elements is higher than 70.9% after decoupling. Please note that the proposed scheme is also applicable for the compact patch antenna arrays with high-coupling levels, such as −9 dB. This can be readily demonstrated by following the proposed design procedure, which is not detailed for brevity.

Other than the specified antenna concept in this article, the proposed aperture-loaded configuration can be extended or varied when facing different demands, discussed as follows.

1) The patch element utilized in this article is pin-fed, and additional aperture structures are essential for decoupling purposes. As for aperture-coupled patch antenna arrays, there already has an aperture loaded in between each feeding line and radiating patch. Thus, the decoupling path can be generated and adjusted by tuning the distance between the feeding line of an element to the feeding aperture of the adjacent element without loading additional apertures. This is of great value to millimeter-wave applications.

2) For the coupling suppression between different sub-arrays with independent transceivers, the proposed method also shows the potential value. We can suppress the strongest coupling between the elements which are normally positioned closest but belong to the different sub-arrays by using the scheme, and then the overall coupling level between the sub-arrays would be reduced.

3) Investigation of a coupling aperture with specified shapes is also an interesting topic to further improve the decoupling bandwidth. For aperture-coupling patch antennas, it has been widely studied to increase the impedance bandwidth of the antennas by using different aperture shapes, such as butterfly- and H-shapes. Similarly, by changing the shape of the decoupling aperture from rectangular to some special ones, the decoupling bandwidth may be improved.

VII. Conclusion

In large-scale antenna arrays for wide-angle scanning applications, it is of great importance to suppress the mutual coupling among the antenna elements. Otherwise, the active impedance matching performance of each element would be significantly influenced, leading to a strong degradation of the maximum scanning angle, peak gain, or scanning accuracy. To deal with this issue, a decoupling method based on aperture loading for large-scale patch antenna arrays is proposed and investigated in this article. Particularly, a novel method that can be simplified implemented by merely loading small apertures on the feeding line of every element, is proposed and studied to generate the additional cancellation path. As verified and discussed in this article, the proposed scheme has a higher potential value in simplifying the decoupling structure, reducing the design complexity, and improving the decoupling bandwidth, compared to the existed network-based decoupling approaches. Moreover, owing to the specified and simple decoupling principle, the proposed scheme works not only for Sub-6 GHz but also for millimeter-wave antennas, making it to be highly attractive for future applications.

References

[1] X. Chen, S. Zhang, and Q. Li, "A review of mutual coupling in MIMO systems," *IEEE Access*, vol. 6, pp. 24706-24719, 2018.

[2] K.-D. Xu, H. Luyen, and N. Behdad, "A decoupling and matching network design for single- and dual-band two-element antenna arrays," *IEEE Trans. Microw. Theory Techn.*, vol. 68, no. 9, pp. 3986-3999, Sep. 2020.

[3] J. Sui and K.-L. Wu, "A general T-stub circuit for decoupling of two dual-band antennas," *IEEE Trans. Microw. Theory Techn.*, vol. 65, no. 6, pp. 2111-2121, Jun. 2017.

[4] K. Qian, L. Zhao, and K.-L. Wu, "An LTCC coupled resonator decoupling network for two antennas," *IEEE Trans. Microw. Theory Techn.*, vol. 63, no. 10, pp. 3199-3207, Oct. 2015

[5] H. Meng and K.-L. Wu, "An LC decoupling network for two antennas working at low frequencies," *IEEE Trans. Microw. Theory Techn.*, vol. 65, no. 7, pp. 2321-2329, Jul. 2017.

[6] Y.-F. Cheng and K.-K. M. Cheng, "A novel dual-band decoupling and matching technique for asymmetric antenna arrays," *IEEE Trans. Microw. Theory Techn.*, vol. 6, no. 5, pp. 2080-2089, May 2018.

[7] B. Wang, Y. Chang, and Y. Sun, "Performance of the large-scale adaptive array antennas in the presence of mutual coupling," *IEEE Trans. Antennas Propag.*, vol. 64, no. 6, pp. 2236-2245, Jun. 2016.

[8] K.-H. Chen and J.-F. Kiang, "Effect of mutual coupling on the channel capacity of MIMO systems," *IEEE Trans. Veh. Technol.*, vol. 65, no. 1, pp. 398-403, Jan. 2016.

[9] L. Savy and M. Lesturgie, "Coupling effects in MIMO phased array," in *Proc. IEEE Radar Conf.* (*RadarConf*), Philadelphia, PA, USA, May 2016, pp. 1-6.

[10] K.-L. Wu, C. Wei, X. Mei, and Z.-Y. Zhang, "Array-antenna decoupling surface," *IEEE Trans. Antennas Propag.*, vol. 65, no. 12, pp. 6728-6738, Dec. 2017.

[11] Y.-M. Zhang, S. Zhang, J.-L. Li, and G. F. Pedersen, "A wavetrap-based decoupling technique for 45°-polarized MIMO antenna arrays," *IEEE Trans. Antennas Propag.*, vol. 68, no. 3, pp. 2148-2157, Mar. 2020.

[12] Y.-M. Zhang, S. Zhang, J.-L. Li, and G. F. Pedersen, "A transmission-line-based decoupling method for MIMO antenna arrays," *IEEE Trans. Antennas Propag.*, vol. 67, no. 5, pp. 3117-3131, May 2019.

[13] C. Wei, Z.-Y. Zhang, and K.-L. Wu, "Phase compensation for decoupling of large-scale staggered dual-polarized dipole array antennas," *IEEE Trans. Antennas Propag.*, vol. 68, no. 4, pp. 2822-2831, Apr. 2020.

[14] M. Li, B. G. Zhong, and S. W. Cheung, "Isolation enhancement for MIMO patch antennas using near-filed resonators as coupling-mode transducers," *IEEE Trans. Antennas Propag.*, vol. 67, no. 2, pp. 755-764, Feb. 2019.

[15] J. Tang, F. Faraz, X. Chen, Q. Zhang, Q. Li, Y. Li, and S. Zhang, "A Metasurface Superstrate for mutual coupling reduction of large antenna arrays," *IEEE Access*, vol. 8, pp. 126859-126867. 2020.

[16] K. S. Vishvaksenan, K. Mithra, R. Kalaiarasan and K. S. Raj, "Mutual Coupling Reduction in Microstrip Patch Antenna Arrays Using Parallel Coupled-Line Resonators," *IEEE Antennas Wireless Propag. Lett.*, vol. 16, pp. 2146-2149, 2017.

[17] L. Zhao and K.-L. Wu, "A decoupling technique for four-element symmetric arrays with reactively loaded dummy elements," *IEEE Trans. Antennas Propag.*, vol. 62, no. 8, pp. 4416-4421, Aug. 2014.

[18] L. Yang, M. Fan, F. Chen, J. She, and Z. Feng, "A novel compact electromagnetic-bandgap (EBG) structure and its applications for microwave circuits," *IEEE Trans. Microw. Theory Techn.*, vol. 53, no. 1, pp. 183-190, Jan. 2005.

[19] Y.-M. Zhang, S. Zhang, and G. F. Pedersen, "A simple and wideband decoupling method for antenna array applications," in *2020 International Workshop on Antenna Technology (iWAT)*, 2020, pp. 1-4.

[20] J. Wen, X. Yang, C. Liu and X. Liu, "Decoupling multi-element patch arrays using waveguided band-gap structure," *2017 International Applied Computational Electromagnetics Society Symposium (ACES)*, Suzhou, 2017, pp. 1-2.

[21] K. Wei, J. Li, L. Wang, Z. Xing and R. Xu, "Mutual coupling reduction by novel fractal defected ground structure bandgap filter," *IEEE Trans. Antennas Propag.*, vol. 64, no. 10, pp. 4328-4335, Oct. 2016.

[22] D. Gao, Z. -X. Cao, S. -D. Fu, X. Quan and P. Chen, "A novel slot-array defected ground structure for decoupling microstrip antenna array," *IEEE Trans. Antennas Propag.*, vol. 68, no. 10, pp. 7027-7038, Oct. 2020.

[23] H. Lin, Q. Chen, Y. Ji, X. Yang, J. Wang, and L. Ge, "Weak-field-based self-decoupling patch antennas," *IEEE Trans. Antennas Propag.*, vol. 68, no. 6, pp. 4208-4217, Jun. 2020.

[24] J. Kornprobst, T. J. Mittermaier, R. A. M. Mauermayer, G. F. Hamberger, M. G. Ehrnsperger, B. Lehmeyer, M. T. Ivrlac, U. Imberg, T. F. Eibert, and J. A. Nossek, "Compact uniform circular quarter-wavelength monopole antenna arrays with wideband decoupling and matching networks," *IEEE Trans. Antennas Propag.*, early published. DOI: 10.1109/TAP.2020.3016422

[25] M. Li, M. Wang, L. Jiang, and K. L. Yeung, "Decoupling of antennas with adjacent frequency bands using cascaded decoupling network," *IEEE Trans. Antennas Propag.*, early published, DOI: 10.1109/TAP.2020.3010956

[26] R.-L. Xia, S.-W. Qu, P.-F. Li, D.-Q. Yang, S. Yang, and Z.-P. Nie, "Wide-angle scanning phased array using an efficient decoupling network," *IEEE Trans. Antennas Propag.*, vol. 63, no. 11, pp. 5161-5165, Nov. 2015.

[27] X.-J. Zou, G.-M. Wang, Y.-W. Wang, and H.-P. Li, "An efficient decoupling network between feeding points for multielement linear arrays," *IEEE Trans. Antennas Propag.*, vol. 67, no. 5, pp. 3101-3108, May 2019.

[28] Y.-M. Zhang, Q.-C. Ye, G. F. Pedersen, and S. Zhang, "A simple decoupling network with filtering response for patch antenna arrays," *IEEE Trans. Antennas Propag.*, 2021, DOI:. 10.1109/TAP.2021.3070632

[29] D. M. Pozar, "Microwave network analysis," in *Microwave Engineering*, 4th ed. Hoboken, NJ, USA: Wiley, 2012, ch. 4, pp. 194-202.

Yi-Ming Zhang (S'17-M'19) received the B.S. degree from Central China Normal University in 2008, the M.S. and Ph.D. degrees from University of Electronic Science and Technology of China in 2014 and 2019, respectively. From 2018 to 2019, he was a guest researcher with the Antenna, Propagation and Millimeter-wave Systems (APMS) Section, Aalborg University, Denmark, where he currently works as a postdoctoral researcher.
Dr. Zhang serves as the reviewer of the IEEE and IET series journals in antenna-design field. His current research interests include massive MIMO antenna, single-channel full-duplex antenna, filtering antenna, OAM antenna, and passive RF and microwave components.

Shuai Zhang (SM'18) received the B.E. degree from the University of Electronic Science and Technology of China, Chengdu, China, in 2007 and the Ph.D. degree in electromagnetic engineering from the Royal Institute of Technology (KTH), Stockholm, Sweden, in 2013. After his Ph.D. studies, he was a Research Fellow at KTH. In April 2014, he joined Aalborg University, Denmark, where he currently works as Associate Professor. In 2010 and 2011, he was a Visiting Researcher at Lund University, Sweden and at Sony Mobile Communications AB, Sweden, respectively. He was also an external antenna specialist at Bang & Olufsen, Denmark from 2016-2017. He has coauthored over 50 articles in well-reputed international journals and over 15 (US or WO) patents. His current research interests include: mobile terminal MMwave antennas, biological effects, CubeSat antennas, Massive MIMO antenna arrays, UWB wind turbine blade deflection sensing, and RFID antennas.